Aerosol radiative forcing over tropical Indian Ocean: Modulation by sea-surface winds

S. K. Satheesh

Centre for Atmospheric and Oceanic Sciences, Indian Institute of Science, Bangalore 560 012, India

It is now clearly understood that atmospheric aerosols have a significant impact on climate because of their important role in modifying the incoming solar and outgoing IR radiation. Recent investigations over the tropical Indian Ocean have shown that the single largest natural contributor of the aerosol visible optical depth are sea-salt aerosols (more than 50% of the natural). It is well known that sea-salt aerosol concentration depends on the sea-surface wind speed[1]. In this paper, the reduction of surface reaching solar flux and increase in the top of the atmosphere (TOA)-reflected solar flux due to the presence of sea-salt aerosols are estimated as a function of wind speed and their role on the radiative forcing and its implications are examined. It is shown that in cloudy conditions over the ocean, the effect of sea-salt is to partly offset the positive forcing (heating) by soot aerosol. The surface and TOA forcing by sea-salt aerosols are as high as -6.1 W m^{-2} and -5.8 W m^{-2} respectively (at high wind conditions), which are about 20% and 60%, respectively of the total aerosol forcing (for a mean aerosol optical depth of 0.4) over tropical northern Indian Ocean. Over pristine regions of the Southern Hemisphere where anthropogenic influence is minimal, forcing is mainly determined by the surface wind speed. Results show that the algorithms for the retrieval of aerosol properties and sea-surface temperature (SST) from satellite data should take into account the changes in aerosol chemical composition with changes in sea-surface wind speed.

ABOUT 30–35% of the global aerosols produced are contributed by the oceans. The major component of oceanic aerosol is sea-salt. Sea-salt particles form the single largest contributor of global aerosol population[1,2]. Sea-salt aerosols are produced over the sea, mainly by the processes associated with the bursting of white-cap bubbles. Extensive measurements of sea-salt aerosols have revealed that the concentration of sea-salt aerosols depends strongly on wind speed at the sea surface and increases exponentially with increase in wind speed[1–4]. After production, the sea-water droplet starts evaporating in order to maintain equilibrium with the ambient relative humidity. Depending on the ambient relative humidity, the droplet can exist either as solution droplet or crystalline solid. The sea-salt aerosols are hygroscopic in nature and hence they act as condensation sites for the formation of cloud droplets. Thus more aerosols produce more cloud droplets, which in turn increases the reflectivity (albedo) of clouds. Also for a given amount of water vapour, more aerosols mean a decrease in the effective radius of cloud droplets (water vapour availability per aerosol is less when aerosol number is more), which in turn increases the lifetime of clouds and reduces precipitation[5].

The chemical composition of aerosols determines its complex refractive indices, which in turn determine its radiative effects. The chemical composition of aerosols over the oceans depends on a number of factors, including the proximity to the continents, synoptic meteorology, local wind conditions, etc. The radiative effects of aerosols are very sensitive to changes in chemical composition. Investigations over the Indian Ocean[6] have shown that the presence of aerosols (corresponding to an optical depth of unity) decreases the surface-reaching solar flux by 70 to 75 W m^{-2} and increases the top of the atmosphere (TOA) reflected flux by 20 to 25 W m^{-2}. Since the sea-salt aerosol concentration depends strongly on the sea-surface wind speed, any local change in winds (aerosol species other than sea-salt remain constant with local winds) can change the chemical composition of composite aerosol, which in turn can change the radiative forcing. In this paper, we examine the role of sea-surface winds in modulating the aerosol radiative forcing (on a regional scale) over the ocean.

Wind dependence of aerosol properties over oceans

Aerosol optical depth

Observations over tropical Indian Ocean have shown that aerosol optical depth (which is a measure of atmospheric transmittance defined such that an optical depth of unity results in an exponential-fold decrease in surface solar flux) increases with sea-surface average wind speed following an exponential relation of the form[1],

$$\tau_a = \tau_0 \exp(bU), \quad (1)$$

where τ_a is the aerosol optical depth at wind speed U, b is

e-mail: satheesh@caos.iisc.ernet.in

a constant called 'wind index' and τ_0 is aerosol optical depth at $U = 0$. Moorthy *et al.*[1] observed that the value of b depends on the wavelength; $b = 0.12$ for $\lambda = 0.5$ μm and $b = 0.18$ for $\lambda = 1.02$ μm. The spectral values of the index b are given in Table 1. Since the production of aerosol species other than sea-salt does not depend on wind speed, the enhancement in aerosol optical depth is attributed to the local production of sea-salt aerosols by the action of wind[1]. Equation (1) is valid when air mass is mainly of marine origin or has a long marine history (not directly influenced by any continental sources)[1]. While deriving eq. (1), aerosol optical depth measurements farther than 1000 km only were used. As such, the equation represents local production of sea-salt aerosols.

The aerosol measurements over tropical Indian Ocean have revealed[7] that sulphate contributes about 29% to aerosol optical depth, sea-salt about 17%, mineral dust about 15%, and the inferred soot, organics and fly ash contribute 11, 20 and 8%, respectively. This observation is for a mean wind speed of 4 m s^{-1}. This is based on measurements carried out at Kaashidhoo Climate Observatory (KCO) (4.9°N, 73.4°E), Republic of Maldives. As wind speed increases, the sea-salt aerosol optical depth increases exponentially, according to eq. (1). An increase in wind speed over a remote marine location does not necessarily mean an increase in wind speed at the source location (several thousand kilometres away) or its pathway to the destination. Thus it is assumed that the concentration of different aerosol species, except sea-salt, is in a steady state and the concentration is independent of changes in local wind speed. It should be noted that the enhancement in sea-salt aerosols is only on a local scale. The per cent contribution of different aerosol components to the total optical depth measured at KCO at a mean wind speed of 4 m s^{-1} is shown in Figure 1. As wind speed increases, the sea-salt aerosol concentration increases, while the other aerosol species remain the same. Thus the composite aerosol concentration also increases (due to sea-salt aerosol enhancement) and as a result increase in wind speed increases the per cent contribution of sea-salt aerosol optical depth. At $U = 4$ m s^{-1} (Figure 1), only 17% of the aerosol optical depth is contributed by sea-salt. Taking the KCO model and 17% of the aerosol optical depth at 4 m s^{-1} (0.2 at 500 nm), the sea-salt optical depth is ~ 0.034. Now the sea-salt optical depth is allowed to increase with wind speed according to eq. (1) and parameters in Table 1, for different wavelengths. The total aerosol optical depth at each wind speed is estimated by adding this enhanced sea-salt optical depth to the composite optical depth due to other species (which are independent of wind speed). The increase in composite aerosol optical depth due to the enhancement in sea-salt optical depth is shown in Figure 2 for $\lambda = 0.5$ μm and $\lambda = 1.02$ μm. At $U = 14$ m s^{-1}, the composite aerosol optical depth is ~ 0.35, in which ~ 0.184 is contributed by sea-salt only (contributes more than half) (Figure 3). This is due to the selective enhancement of sea-salt aerosols with wind speed, while other components remain the same. It should be noted that eq. (1) represents the enhancement of sea-salt aerosols in response to increase in sea-surface winds and was derived from a marine location where major part of the aerosol was contributed by sea-

Table 1. Spectral values of the wind index[1]

Wavelength (μm)	Wind index, b
0.40	0.12
0.50	0.12
0.75	0.14
0.85	0.17
1.02	0.18

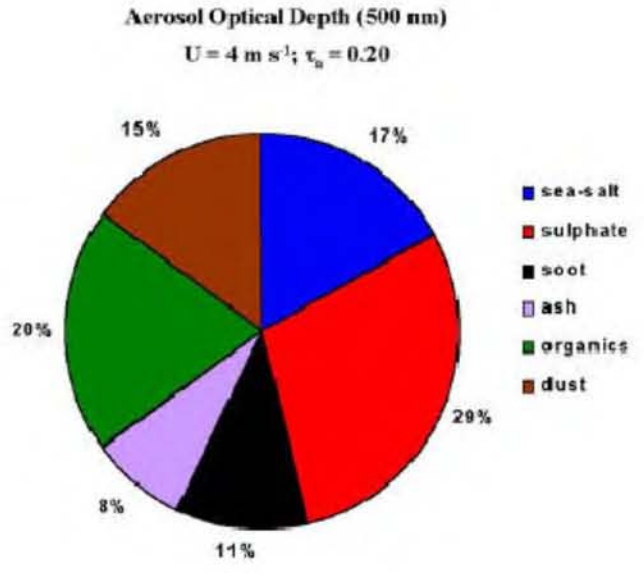

Figure 1. Contribution of various aerosol species to the aerosol optical depth at 500 nm for a wind speed of 4 m s^{-1}.

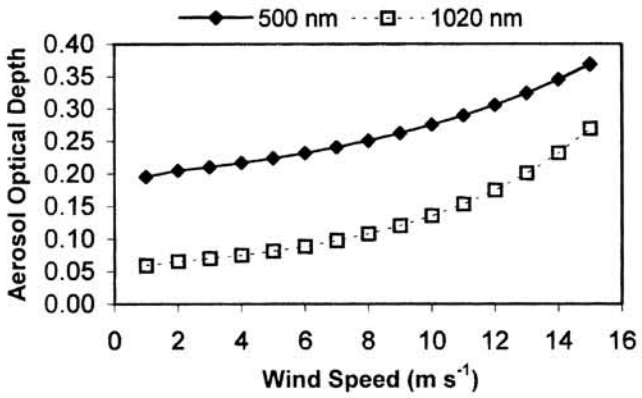

Figure 2. Enhancement of aerosol optical depth with wind speed at two representative wavelengths.

salt. There, an increase in sea-salt concentration would reflect on the total optical depth at the same rate. In the present case, sea-salt is only one among the various species and contributes only 17% to the composite aerosol optical depth. Hence the optical depth of a composite aerosol will not increase by the same amount as given by eq. (1), but only to a lesser level (determined by the increase in the share of sea-salt to the total), as seen in Figure 2.

Angstrom coefficients

A simple way of representing the spectral variation of aerosol optical depth is by using the Angstrom power law given by,

$$\tau_a = \beta\lambda^{-\alpha}, \quad (2)$$

where α is the wavelength exponent, β is the turbidity parameter and λ is the wavelength in μm. The value of α depends on the ratio of the concentration of large to small aerosols and β represents the total aerosol loading in the atmosphere[8]. The values of α and β are obtained by least-square fitting of the spectral optical depths in a log–log scale. The mean aerosol spectral optical depth at KCO (measured at a mean wind speed of 4 m s^{-1}) was used to simulate the spectral optical depths at different wind speeds from 0 to 15 m s^{-1} using eq. (1) and coefficients given in Table 1. At each wind speed the sea-salt optical depth was estimated using eq. (1) and the model was re-normalized. Thus the aerosol spectral optical depth was estimated at different wind speeds from 0 to 15 m s^{-1}. The values of α and β estimated from spectral aerosol optical depths at different wind speeds are shown in Figure 4 *a*. From Table 1 it is clear that the super-micron ($r > 1$ μm) aerosols (the effect of which is more at near-IR wavelengths compared to visible, according to Mie scattering theory) are produced more by the action of wind compared to sub-micron ($r < 1$ μm) aerosols (the effect of which is more at visible wavelengths compared to near-IR). Since α is the slope of the spectral variation in log–log scale, the selective enhancement of the near IR aerosol optical depth with speed decreases the value of α (Figure 4 *a*). Since β is equal to $\tau_a = 1$ μm (from eq. (2)), it increases exponentially with wind speed, according to eq. 1 (Figure 4 *a*).

Single scattering albedo

The single scattering albedo (SSA) is a measure of the effectiveness of scattering in extinction and is defined as the ratio of scattering coefficient to extinction coefficient. Extinction is the combined effect of scattering and absorption. The SSA depends on the chemical composition and by definition a completely scattering aerosol has an SSA of 1.0 and a completely absorbing aerosol has an SSA of 0.0. The composite SSA of the aerosol system is

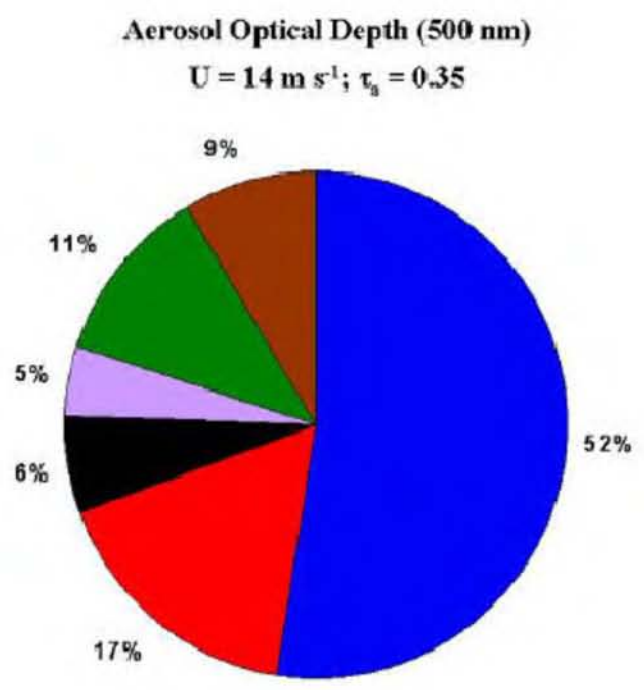

Figure 3. Contribution of various aerosol species to the aerosol optical depth at 500 nm for a wind speed of 14 m s^{-1} (colour scheme for different aerosol types is the same as that in Figure 1).

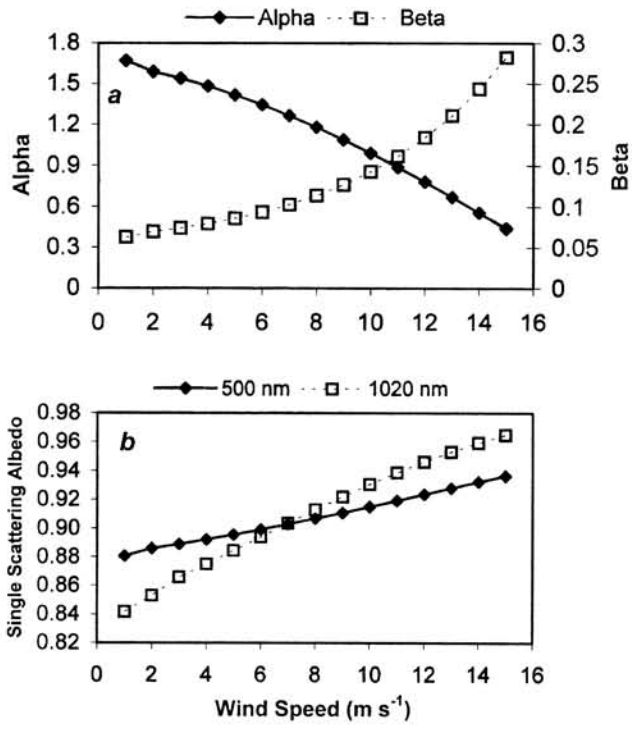

Figure 4. Variation of (*a*) α and β and (*b*) single scattering albedo (at two representative wavelengths), with wind speed.

the weighted average (weighted by the extinction coefficient) of SSA of individual aerosol species. The SSA of different aerosol species is taken from Hess *et al.*[9] and is given in Table 2. The composite aerosol SSA is given by,

$$\omega_\lambda = \left(\frac{\omega_{1\lambda} E_{1\lambda} + \omega_{2\lambda} E_{2\lambda} + \omega_{3\lambda} E_{3\lambda} + \ldots}{E_{1\lambda} + E_{2\lambda} + E_{3\lambda} + \ldots} \right), \quad (3)$$

where $\omega_{1\lambda}$, $\omega_{2\lambda}$, $\omega_{3\lambda}$, etc. are the SSA and $E_{1\lambda}$, $E_{2\lambda}$, $E_{3\lambda}$, etc. are the extinction coefficients of individual aerosol species. As the wind speed increases, the sea-salt aerosol optical depth increases exponentially (according to eq. (1)), whereas those of the other components remain constant with wind speed. The SSA at two representative wavelengths (visible and near-IR) estimated using eq. (3) is, shown in Figure 4 *b* for different wind speeds. The increase in SSA is more at near-IR wavelengths because the increase in sea-salt optical depth at near-IR wavelength is more, and more weight is given to the sea-salt SSA (which is 1.0) while estimating the composite SSA (according to eq. (3)).

Radiative transfer model

The aerosol spectral optical depth and spectral SSA described above are incorporated in a Monte Carlo radiative transfer (RT) model[10] to estimate the aerosol impact (forcing) on the broadband fluxes at the surface and the TOA. In this paper, the term, 'aerosol radiative forcing' represents the effect of aerosols on the radiative fluxes. The effect of aerosols on TOA radiative fluxes is the TOA radiative forcing; on surface fluxes is the surface radiative forcing, and the difference between the two is the atmospheric radiative forcing. In all these cases the aerosol forcing is the difference in solar radiation with and without aerosols. The aerosol radiative forcing arises from their interaction with solar radiation. The band from 0.2 to 4.0 μm (short wave) is divided into 38 narrow bands. The band centres are more closely spaced in the visible wavelengths compared to infrared wavelengths, as a major fraction of incoming solar radiation is in the visible region. The per cent contribution of different species to the aerosol optical depth and SSA is estimated for these 38 band centers. The radiative transfer model used for the present study allows to treat different aerosol species explicitly in the model. The molecular absorption due to water vapour, CO_2, O_2, and O_3 is taken into account[10]. The zenith angle-dependent ocean albedo (reflectance) is used[11]. Each of the chemical species is treated separately in the Monte Carlo model by using the corresponding phase functions and SSAs for individual species[9]. The phase functions (at 500 nm) of different aerosol species estimated for 70% relative humidity are shown in Figure 5. In the RT model, phase function at three wavelengths is used to represent the 38 bands. The phase function at 500 nm is used to represent the bands from 0.2 to 1.0 μm, that at 1.5 μm is used to represent bands from 1.0 to 2 μm and that at 3 μm is used to represent the bands from 2 to 4 μm. In usual practice, many previous investigations used only one phase function and SSA (normally 500 nm) to represent the whole spectral range. However, depending on the aerosol size distribution, the phase function at different wavelengths also changes significantly. Thus the use of three phase functions and 38 SSAs increases the accuracy of the present study.

Table 2. SSA of various aerosol species[9]

Aerosol type	SSA (500 nm)
Sea-salt	1.0
Sulphate	1.0
Soot	0.23
Dust	0.78
Organics	0.97
Ash	0.96

Aerosol forcing

The parameters estimated for each wind speed bin (1 m s^{-1} interval from 0 to 15 m s^{-1}) are the following.

1. The spectral composite aerosol optical depth for 38 wavelength bands from 0.2 to 4 μm.
2. The per cent contribution to the composite aerosol optical depth of different aerosol species for 38 bands from 0.2 to 4 μm.
3. The spectral SSA for 38 bands from 0.2 to 4 μm.
4. The Angstrom coefficient to interpolate aerosol optical depth within individual wavelength bands.
5. The phase function at 0.5, 1.5 and 3 μm.

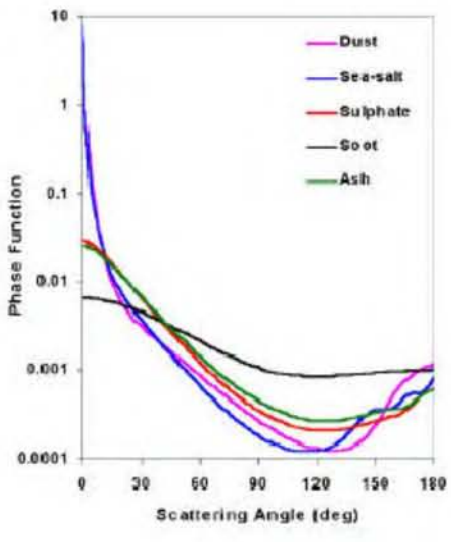

Figure 5. Phase function of various aerosol species at 500 nm.

These parameters are used as input to the RT model for values of wind speed from 0 to 15 m s^{-1}.

For estimating the diurnally averaged aerosol forcing, the estimated flux is subtracted from the average flux with no aerosol[6]. The solar flux at different zenith angles is simulated with and without aerosol in the model. The difference between the solar flux with and without aerosol is the forcing. Since incident solar radiation is maximum around local noon, forcing is also maximum around noon. During the night, there is no incident solar radiation and hence forcing is zero. The diurnal average is obtained by averaging the forcing over a full day (24 h). The aerosol optical depths at 38 wavelength bands are partitioned between various aerosol components according to the corresponding per cent contributions at that wavelength (similar to Figures 1 and 3, for 0.5 μm and 1.02 μm). The aerosol forcing is plotted as a function of aerosol optical depth and the slope of the forcing vs τ_a provided an independent estimate of the aerosol forcing per unit optical depth (called forcing efficiency), which multiplied by the individual τ_a, yields the aerosol forcing for each case[12]. The forcing estimated in this way is free from any offsets (non-zero forcing at zero optical depth) in the model, if present.

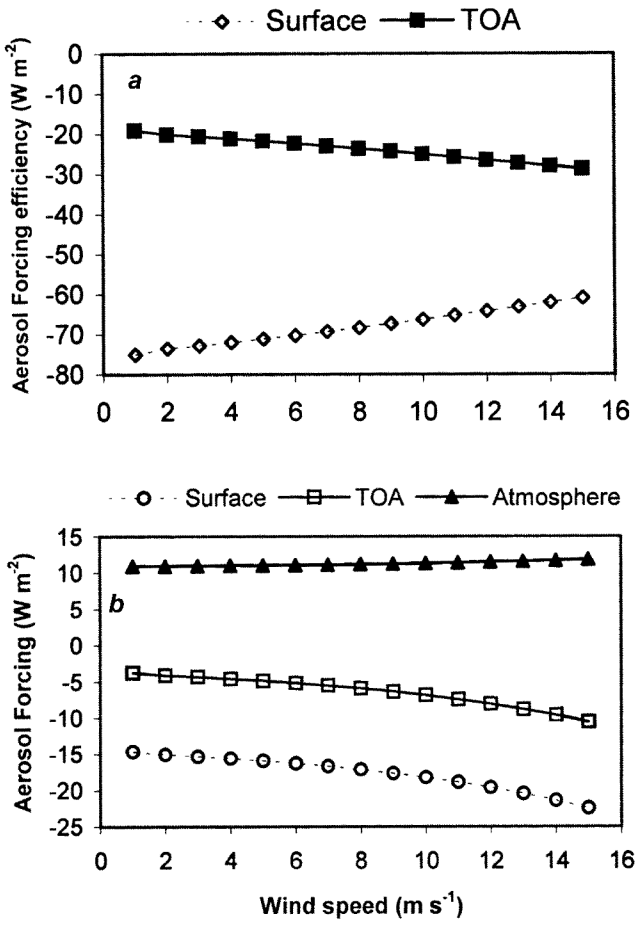

Figure 6. Variation of (*a*) aerosol forcing efficiency, and (*b*) aerosol forcing with wind speed.

The incorporation of aerosol optical properties into the radiative transfer model has shown that aerosol forcing efficiency (which is the aerosol forcing per unit aerosol optical depth) at the surface changes from – 76 to – 62 W m^{-2} and at the TOA from – 20 to – 28 W m^{-2}, as wind speed changes from 0 to 15 m s^{-1} (Figure 6 *a*). Since the aerosol optical depth is constrained as unity, the change is mainly due to the changes in aerosol SSA shown in Figure 4 *b*. Aerosol forcing is the aerosol forcing efficiency multiplied by aerosol optical depth. As wind speed increases, there are two competing effects which determine the aerosol forcing at the surface; they are increase in SSA and increase in optical depth. Increase in SSA decreases the forcing efficiency, whereas increase in optical depth increases the forcing. At the TOA, both increase in SSA and increase in optical depth increase the forcing. The composite aerosol forcing efficiency and aerosol forcing are shown in Figure 6 *a* and *b* as a function of wind speed. The sea-salt aerosol forcing is shown in Figure 7 for $U = 0$ to 15 m s^{-1}. It can be seen that the atmospheric absorption almost remains the same with increased wind speed. This is because of the negligible solar absorption by sea-salt. Thus the increased sea-salt in response to an increase in wind speed from 4 to 14 m s^{-1} increases aerosol surface forcing by ~ 6.2 W m^{-2} and the TOA forcing by ~ 5.8 W m^{-2}. This means that reduction of solar radiation at the sea-surface due to the presence of aerosols is enhanced by increase in wind speed. This may have a consequent impact on sea-surface temperature (SST). The enhancement in forcing at the TOA implies more energy is lost to space due to increased winds, which tend to cool the atmospheric column.

The advantage of the Monte Carlo radiative transfer model is that each aerosol species can be described explicitly. The contributions of the individual aerosol species are estimated by removing the component from the model and subtracting the resulting forcing from the composite forcing. In this way the multiple interactions

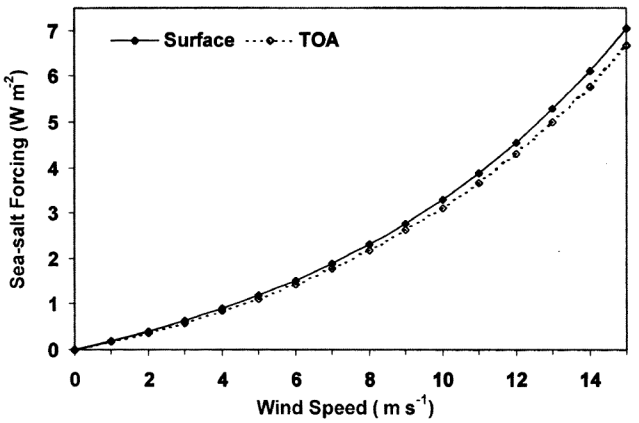

Figure 7. Variation of sea-salt aerosol forcing with wind speed.

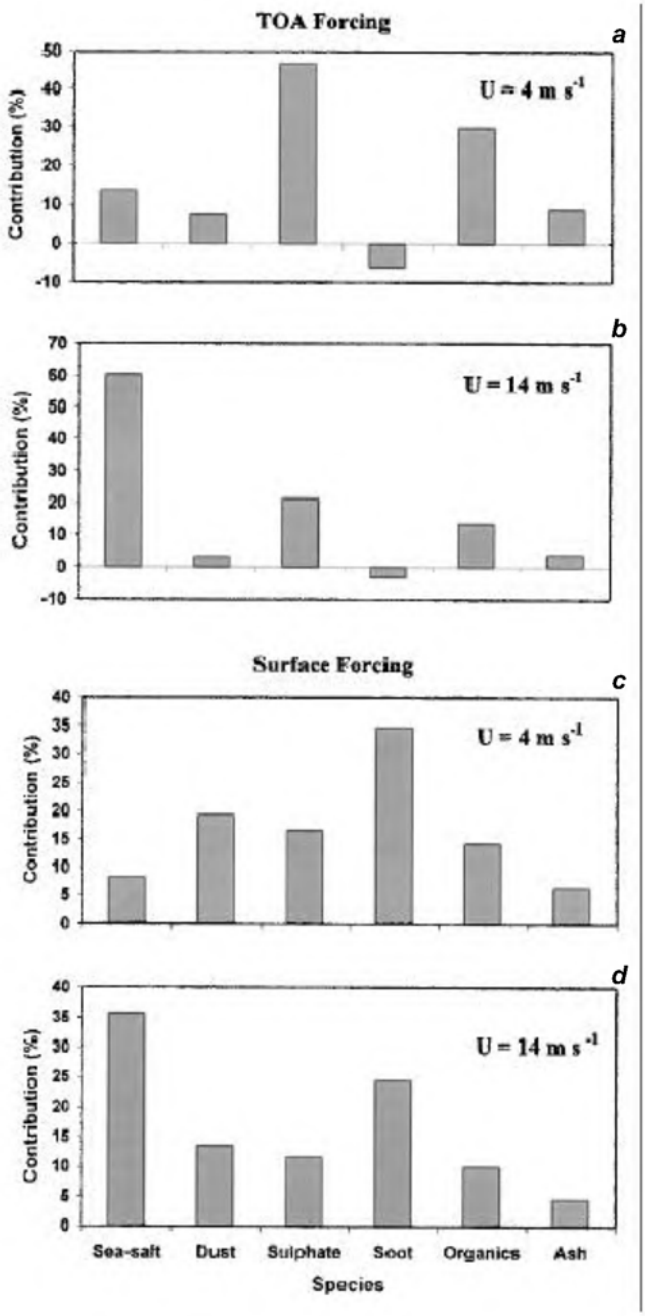

Figure 8. Per cent contribution of various aerosol species to the composite aerosol forcing at the TOA (***a*** and ***b***) and at the surface (***c*** and ***d***). The forcing at $U = 4$ m s^{-1} and $U = 14$ m s^{-1} is shown for each case.

between the other components are taken into account. The contribution of individual aerosol components to the composite forcing is shown in Figure 8. It can be seen that surface wind has a significant role in modifying the chemical composition of aerosols and hence the surface and TOA forcing. As the wind speed increases, the sea-salt concentration and as a result composite aerosol concentration also increase, whereas other aerosol species remain constant. Thus at high wind speeds ($U > 10$ m s^{-1}),

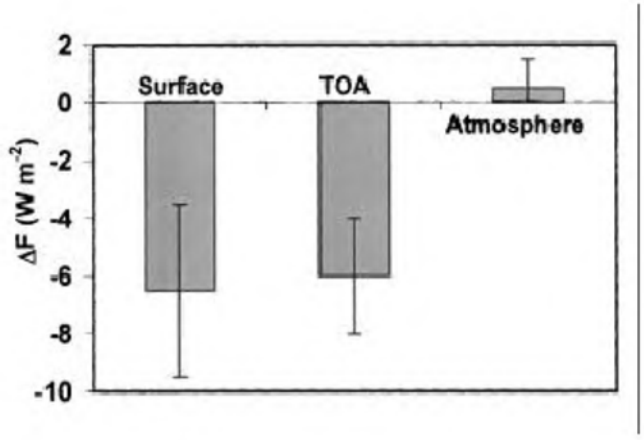

Figure 9. Change in aerosol forcing when wind speed changes from 0 to 14 m s^{-1}.

the sea-salt becomes the dominant contributor to the composite aerosol forcing both at the surface and at the TOA.

The change in aerosol forcing (ΔF) when the wind speed changes from 0 to 14 m s^{-1} is shown in Figure 9. It can be seen that both surface and TOA forcing are comparable in magnitude, and atmospheric absorption due to sea-salt aerosol is very small. Thus the sea-salt aerosols are not contributing much to atmospheric heating by solar radiation. Model estimates of aerosol forcing in clear and cloudy skies have shown that aerosol forcing at the TOA decreases as cloud cover increases and can be positive when cloud coverage exceeds ~ 25% (ref. 13). When a reflecting cloud layer is present, both aerosol scattering and absorption effects are amplified due to the multiple interactions of the radiation reflected back by clouds or between the clouds and the surface[14]. Thus the effect of the sea-salt aerosol is to offset (as the TOA forcing by sea-salt aerosol is negative or in other words cooling) part of the heating by soot aerosols. The NCEP (National Centre for Environmental Prediction) data show that the wind speeds are generally in the range of 10 to 12 m s^{-1} at around 10°S to 15°S, and since anthropogenic influence is minimal in this region; the major determinant of aerosol forcing is sea surface winds. The winds are about 14–16 m s^{-1} (monthly mean) near Somali coast (around 5°N, 50°E, where clear skies are frequent), which indicates significant sea-salt contribution to radiative forcing in this region.

Summary and conclusion

The sea-salt aerosols are produced over the ocean by the action of sea-surface winds. The surface and the TOA forcing by sea-salt aerosols are as high as -6.1 W m^{-2} and -5.8 W m^{-2}, respectively (at high wind conditions with $U = 12$ to 15 m s^{-1}), which are about 20% and 60% respectively, of the total aerosol forcing (for a mean

aerosol optical depth of 0.4) over the tropical northern Indian Ocean. In cloudy conditions over the ocean, the sea-salt aerosols partly offset the TOA positive forcing (heating) by soot aerosol, while complementing the surface forcing. The sea-salt aerosol has a significant role in determining the TOA radiance measured by satellites and hence algorithms for retrieving the aerosol properties from satellites should have wind speed as input to account for the changes in aerosol chemical composition with wind speed. Since sea-salt absorbs in the infrared, the retrieval of SST from satellite data (IR brightness temperature) should take into account the sea-surface wind-speed changes.

1. Moorthy, K. K., Satheesh, S. K. and Krishna Murthy, B. V., *J. Geophys. Res.*, 1997, **102**, 18827–18842.
2. Fitzgerald, J. W., *Atmos. Environ.*, 1991, **25**, 533–545.
3. Lovett, R. F., *Tellus*, 1978, **30**, 358–364.
4. Hoppel, W. A., Fitzgerald, J. W., Frick, G. M. and Larson, R. E., *J. Geophys. Res.*, 1990, **95**, 3659–3686.
5. Ramanathan, V. *et al.*, *J. Geophys. Res.*, 2001 (in press).
6. Satheesh, S. K. and Ramanathan, V., *Nature*, 2000, **405**, 60– 63.
7. Satheesh, S. K. *et al.*, *J. Geophys. Res.*, 1999, **104**, 27421–27440.
8. Shaw, G. E., Reagan, J. A. and Herman, B. M., *J. Appl. Meteorol.*, 1973, **12**, 374–380.
9. Hess, M., Koepke, P. and Schult, I., *Bull. Am. Meteorol. Soc.*, 1998, **79**, 831–844.
10. Podgorny, I. A., Conant, W. C., Ramanathan, V. and Satheesh, S. K., *Tellus*, 2000, **B52**, 947–958.
11. Breigleb, B. P., Minnis, P., Ramanathan, V. and Harrison, E., *J. Climat. Appl. Meteorol.*, 1986, **25**, 214–226.
12. Jayaraman, A., Lubin, D., Ramachandran, S., Ramanathan, V., Woodbridge, E., Collins, W. and Zalpuri, K. S., *J. Geophys. Res.*, 1998, **103**, 13827–13836.
13. Podgorny, I. A. and Ramanathan, V., *J. Geophys. Res.*, 2001 (in press).
14. Heintzenberg, J. *et al.*, *Beitr. Phys. Atmos.*, 1997, **70**, 249–263.

ACKNOWLEDGEMENTS. I thank Prof. J. Srinivasan, Centre for Atmospheric and Oceanic Sciences, Indian Institute of Science, Bangalore and Dr K. Krishna Moorthy, Space Physics Laboratory, Thiruvanathapuram for valuable suggestions and discussion. I also thank Prof. V. Ramanathan, Centre for Atmospheric Sciences, Scripps Institution of Oceanography, San Diego for providing the radiative transfer model. Thanks are also due to Ms Vidyunmala for providing the NCEP wind data.

Received 18 August 2001; revised accepted 10 October 2001

Impact of Deccan volcanism on deep crustal structure along western part of Indian mainland and adjoining Arabian Sea

A. P. Singh

National Geophysical Research Institute, Uppal Road, Hyderabad 500 007, India

To understand the magmatic processes originating in the deep mantle and their impact on the lower crustal level, the conspicuous gravity anomalies observed over the western part of Indian mainland and contiguous Arabian Sea were modelled, integrating the available seismic information. The unified 2D and subsequent 3D density modelling of the Narmada–Tapti region suggests a 15–20 km thick high-density (3.02 g cm^{-3}) accreted igneous layer at the base of the crust. The thickness of this layer varies from about 8 km near Multai to about 16 km beneath the central part and about 24 km beneath Navsari in the westernmost part of the Narmada–Tapti region. Similarly, a 7–11 km thick accreted igneous layer characterizes the Eastern Basin, including the Laxmi Ridge (LR) in the northeastern Arabian Sea. Thickness of this layer varies from about 4 km beneath the northwestern part to about 11 km beneath the central part of the LR. The extension of this layer towards the southeast and ultimate connection with the Chagos–Laccadive Ridge makes the western boundary of the magmatic crustal accretion along the west coast of India. The Konkan Coast, further down south, is also characterized by a ca. 3 km thick and about 40 km wide accreted igneous layer at the base of the crust along the coastline. It is suggested that this widespreading magmatic underplating along the western part of Indian land mass and adjoining Arabian Sea is the imprint of the Deccan magmatism caused by the deep mantle plume, when the northward migrating Indian plate passed over the Reunion hot spot.

THE western part of Indian mainland and adjoining Arabian Sea distinguishes itself distinctly from its counterpart in the east. The region suffered most in the period after the break-up of Gondwanaland. During this time it passed through an extremely dynamic phase, marked by an extensive plate reorientation and massive volcanism (Figure 1). Several micro-continents such as the Madagascar and the Sechelles-Mascarene block may have existed along the west coast, before being broken away from the mainland. Several hidden tectonic features

e-mail: apsingh_ngri@yahoo.com